Clim Dyn (2017) 49:1547–1566
DOI 10.1007/s00382-016-3397-8

High resolution projections for the western Iberian coastal low level jet in a changing climate

Pedro M. M. Soares[1] · Daniela C. A. Lima[1] · Rita M. Cardoso[1] · Alvaro Semedo[1,2]

Received: 20 October 2015 / Accepted: 9 October 2016 / Published online: 19 October 2016

Abstract The Iberian coastal low-level jet (CLLJ) is one of the less studied boundary layer wind jet features in the Eastern Boundary Currents Systems (EBCS). These regions are amongst the most productive ocean ecosystems, where the atmosphere–land–ocean feedbacks, which include marine boundary layer clouds, coastal jets, upwelling and inland soil temperature and moisture, play an important role in defining the regional climate along the sub-tropical mid-latitude western coastal areas. Recently, the present climate western Iberian CLLJ properties were extensively described using a high resolution regional climate hindcast simulation. A summer maximum frequency of occurrence above 30 % was found, with mean maximum wind speeds around 15 ms^{-1}, between 300 and 400 m heights (at the jet core). Since the 1990s the climate change impact on the EBCS is being studied, nevertheless some lack of consensus still persists regarding the evolution of upwelling and other components of the climate system in these areas. However, recently some authors have shown that changes are to be expected concerning the timing, intensity and spatial homogeneity of coastal upwelling, in response to future warming, especially at higher latitudes, namely in Iberia and Canaries. In this study, the first climate change assessment study regarding the Western Iberian CLLJ, using a high resolution (9 km) regional climate simulation, is presented. The properties of this CLLJ are studied and compared using two 30 years simulations: one historical simulation for the 1971–2000 period, and another simulation for future climate, in agreement with the RCP8.5 scenario, for the 2071–2100 period. Robust and consistent changes are found: (1) the hourly frequency of occurrence of the CLLJ is expected to increase in summer along the western Iberian coast, from mean maximum values of around 35 % to approximately 50 %; (2) the relative increase of the CLLJ frequency of occurrence is higher in the north off western Iberia; (3) the occurrence of the CLLJ covers larger areas both latitudinal and longitudinal; (4) the CLLJ season is lengthened extending to May and September; and, (5) there are shifts for higher occurrences of higher wind speeds and for the jet core to occur at higher heights.

Keywords Climate change · Regional climate modelling · Coastal low-level wind jet · Iberian Peninsula · WRF

1 Introduction

Coastal low-level jets (henceforth CLLJ or coastal jets) have been identified as important features along all eastern boundary current systems (EBCS; Winant et al. 1988; Ranjha et al. 2013), in the regions between the semi-permanent ocean anticyclones and the mid-latitude western margins of continents: along the California (Winant et al. 1988; Burk and Thompson 1996; Parish 2000) and the Canary (Winant et al. 1988; Soares et al. 2014) currents in the northern hemisphere, and along the Peru-Humboldt (Garreaud and Muñoz 2005; Garreaud et al. 2011), Benguela (Nicholson

Electronic supplementary material The online version of this article (doi:10.1007/s00382-016-3397-8) contains supplementary material, which is available to authorized users.

✉ Pedro M. M. Soares
pmsoares@fc.ul.pt

[1] Instituto Dom Luiz, Faculdade de Ciências, Universidade de Lisboa, Campo Grande, Ed. C8 (3.26), 1749-016 Lisbon, Portugal

[2] Department of Water Science and Engineering, UNESCO-IHE, Delft, The Netherlands

2010) and West Australia (Stensrud 1996) currents in the southern hemisphere. The existence of a CLLJ in the Arabian Sea, along the coasts of Yemen and Oman (Ranjha et al. 2013, 2015) is an exception to this pattern, since it does not occur along an EBCS in a western continental coast. The Oman CLLJ is the result of the interaction between the summer South Asian Monsoon and the Findlater jet (also known as Somali jet; Findlater 1969). Lately, several studies revealed the existence of an Iberian CLLJ, connected with the North African CLLJ (Ranjha et al. 2013; Soares et al. 2014).

Coastal jets features are related to low-level winds of high intensity within the shallow well-mixed marine atmospheric boundary layer (MABL). The synoptic pattern, determined by the off-shore anticyclone and by the inland thermal low pressure, forces an along-shore flow that is vertically compressed by the subsidence associated both to the anticyclone and the continental thermal lows. The latter are regionally established by the land–ocean temperature contrast, which forces an onshore sea-breeze that is deflected by the Coriolis force, enhancing an along-shore wind component. Additionally, the coastal topography, often higher than the well mixed inversion capped MABL, blocks the cross-shore component of the flow and channels it along the coast, locally modulating it by coastal and orographic features, like capes, bays, valleys and mountains (Tjernström 1999; Pomeroy and Parish 2001). Typically the CLLJs core (wind speed maxima) is located near the MABL inversion (usually below the first atmospheric kilometre), and can present wind speeds higher than 15 ms^{-1}, with horizontal offshore extensions exceeding hundreds of kilometres, restricted by the Rossby radius of deformation (Overland 1984).

The relevance of CLLJs for the regional climate has been documented in several studies. The Benguela coastal jet in Africa feedbacks positively with local upwelling and is believed to enhance the Namibe desert aridity (Lettau 1978; Nicholson 2010). Moreover, the interaction of the CLLJs and SSTs in the Benguela coast and adjacent Atlantic sectors seems to have a significant influence on the rainfall variability of other African regions, like the Sahel (Lamb and Peppler 1992; Reason and Rouault 2006; Nicholson and Webster 2007), in East Africa (Goddard and Graham 1999; Nicholson and Entekhabi 1987) and in western equatorial Africa (Balas et al. 2007). In the cases of the Californian CLLJ (e.g. Burk and Thompson 1996; Parish 2000) and of the Peruvian–Chilean CLLJ (Garreaud and Muñoz 2005) a similar role of CLLJs takes place outlining some of the most arid regional climates in the world (Lettau 1978). Helfand and Schubert (1995) highlights the CLLJ role in the regional moisture transport over California, showing its blocking effect, by inhibiting the low-level advection of moisture into the continent from the west. But, in the southern region of the Gulf of California, Douglas (1995) showed that the California CLLJ is responsible for significant moisture episodes connected to the North American monsoon. Webster and Hoyos (2004) acknowledged the low-level jet as an important component of the Indian monsoon system and its role in intra-seasonal and inter-annual variabilities.

Coastal jets are strongly linked to regional ocean dynamics (Beardsley et al. 1987) forcing coastal upwelling and nutrient-enriched waters at the coast. The dominant forcing mechanisms of the SST cooling during CLLJs is a mixture of seaward advection of temperature resulting from Ekman transport, air-sea heat exchange, and Ekman-driven coastal divergence (Renault et al. 2009). As a result, the upper thermocline rises towards the surface as the coast is approached. When the upwelling is intense or endures for a sufficient length of time, the thermocline may reach the surface and appears as a front along the coast which travels back and forth depending upon the strength of the upwelling. Observations show that in upwelling regions the Ekman layer thickness is often smaller than in the open ocean, presumably because upwelling brings the thermocline closer to the surface inhibiting wind mixing beyond a depth of 20–30 m (Tomczak and Godfrey 1994). Finally, the upwelling colder SSTs enhance the thermal contrast between land and ocean and feed-back positively on the CLLJs. They are, thus, important for coastal weather and impact directly in many societal activities and economic sectors, like aviation, shipping, fisheries, pollutant and aerosol dispersion, off-shore wind farms, tourism, etc. The societal impacts of coastal jets and its role in the definition of regional climates enforces the need for the understanding of how CLLJ will change in the context of global warming, consequence of the anthropogenic emissions of greenhouse gases. A warmer climate may lead to an intensification of the positive feedback between CLLJs and coastal upwelling (Bakun 1990), having important implications for local ocean currents and to the inter-connected climatic variability and change, making the EBCS regions particularly vulnerable to the impacts of global climate change (Snyder et al. 2003; Miranda et al. 2013; Bakun et al. 2015). Wang et al. (2015) showed that robust and consistent changes in the timing, intensity and spatial homogeneity of coastal upwelling is expected to occur, in response to future warming, in most EBCS. In fact, three out of four of the EBCS (Canary, Benguela and Humboldt, but not California), reveal consistent changes, by the end of the twenty-first century, in upwelling intensity and duration at high latitudes, resulting in a substantial reduction of the existing latitudinal variation in coastal upwelling. Furthermore, these authors' projections point out to an earlier start and later end of the upwelling season, becoming more intense at high but not low latitudes. Recently, Semedo

et al. (2016) analysed a set of global simulations performed using the EC-EARTH global climate model, for present and future climates. They have shown that significant changes in the frequency of occurrence of CLLJs, most notably for Iberia and Oman, are projected to occur by the end of the twenty-first century (but not for the California CLLJ, which is in agreement with Wang et al. 2015). These studies lead to the need of addressing thoroughly the changes in the Iberian Peninsula CLLJ properties and annual cycle in response to global warming.

The Iberian coastal low-level jet has been referred in a small number of studies (e.g. Relvas and Barton 2002; Hoinka and de Castro 2003; Torres et al. 2003; Alvarez et al. 2008), however none clearly show observational evidence or characterize its main properties. In fact, these studies focus on the on the surface wind and on the wind-driven upwelling (Relvas and Barton 2002; Torres et al. 2003; Alvarez et al. 2008); and on the surface wind and its dependence on the Iberian thermal low (Hoinka and de Castro 2003). Those authors suggest that summer surface wind maxima and its seasonality as a surface indication of the low-level jet presence. Very recently, Monteiro et al. (2016) revealed the first observational evidence of the Iberian coastal low-level jet, through aircraft measurements performed off the Lisbon coast. During a low-level jet event, aircraft measurements showed the local wind maximum at higher levels in a good agreement with numerical simulations. Soares et al. (2014) presented the first high resolution study on the Iberian CLLJ, pointing out that in present climate the Western Iberian CLLJ has a mean maximum wind speed around 15 ms^{-1}, located between 300 and 400 m height, and has a maximum frequency of occurrence, in summer, above 30 % downwind of the main coastal features (Capes Finisterre, Roca and São Vicente). The CLLJ occurrence has a clear annual cycle, with frequencies of occurrence of around 10 % in the intermediate seasons, and being almost inexistent in winter. Furthermore, the coastal jet spatial patterns and frequencies of occurrences have large inter-annual variabilities. As aforementioned, Semedo et al. (2016) projected a jet occurrence growth for Iberia in a warming climate, nevertheless the coarse resolution limits the knowledge of the regional and local details of these changes, indicating the need for higher resolution studies. Semedo et al. (2016) associated this increase to the intensification of the Azores Anticyclone. In fact, Davis et al. (1997) examining a twentieth century surface pressure climatology revealed that the meridional flow has increased over the Atlantic, and Li et al. (2012) projected an intensification of Northern Hemisphere subtropical highs in a warming climate, predominantly caused by an increase in thermal contrast between the land and ocean. This enhanced thermal contrast is expected also to lead to an inland thermal low higher frequency.

In this study, the analysis presented by Soares et al. (2014) is applied to a full set of climate simulations, to examine emerging signals of future changes in the properties of the Western Iberian CLLJ associated with global warming. The simulations were performed using the Weather Research and Forecast (WRF) model, at 9 km resolution, for an historical period (1971–2000) and a future period (2071–2100). This high resolution investigation allows an exhaustive characterization of the expected changes of the Iberian CLLJ by the end of the twenty-first century, regarding the mean properties, the annual cycle and the spatial and temporal variabilities.

2 Data and methods

2.1 WRF climate simulations

As previously referred, Soares et al. (2014) carried out a high resolution numerical study devoted to the characterization of the western Iberia CLLJ for the present climate, using ERA-Interim (Dee et al. 2011) to force the Weather and Research Forecasting (WRF) model (Skamarock et al. 2008) as a regional climate model. In the current study, a full set of high resolution climate simulations is used for historical and future climates, also using the WRF and with a similar set up to the hindcast. The historical run is forced by the EC-EARTH model (Hazeleger et al. 2010) for the period 1971–2000, and the future climate simulation is also forced by EC-EARTH for the 2071–2100 time-slice. The set of simulations encompass two domains, one larger at 27 km resolution, and a nested higher resolution domain at 9 km, both centred in the Iberian Peninsula (Fig. 1a). Since a good representation of the planetary boundary layer is crucial, 49 vertical levels were used, with 20 vertical levels in the boundary layer. The lowest model sigma level is at approximately 10 m of height, the second level at 30 m, and the following distances, between levels, increase by 10 % in the first 1000 m and model top is at 50 hPa. Additionally, and as in the hindcast, the chosen physical parameterizations include the microphysics WSM 6 class single-moment (mp6) scheme by Hong and Lim (2006), the planetary boundary layer scheme of Mellor–Yamada–Janjic (Janjic 2001) and the Betts–Miller–Janjic cumulus scheme (Betts 1986; Betts and Miller 1986; Janjic 1990, 1994, 2000). The simulations use the Noah LSM 4-layer soil temperature, soil and canopy moistures model (Chen and Dudhia 2001). The radiation scheme used relies on the shortwave and longwave schemes (Collins et al. 2004) of the NCAR Community Atmospheric model. These options have been evaluated for inland surface variables, namely, maximum and minimum temperatures and precipitation in mainland Portugal (Soares et al. 2012), Iberian precipitation

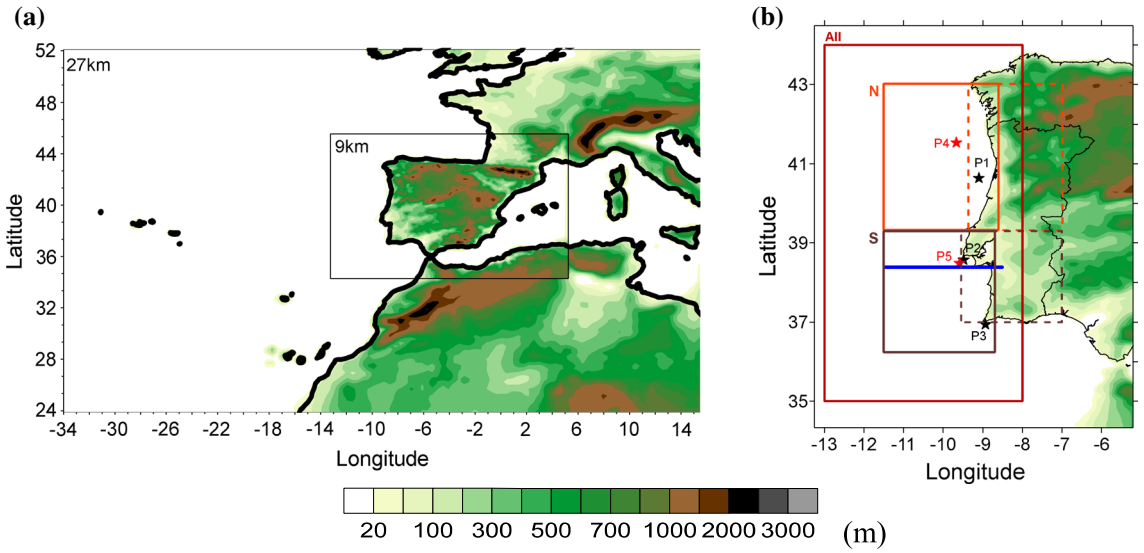

Fig. 1 **a** WRF model domains (27 and 9 km) and correspondent domain topographies. **b** Western Iberian region of interest and orography at 9 km. *Boxes* (*All*, *BoxN* and *BoxS*) used for regional analysis over land and ocean (*sea boxes* in full contour and *land boxes* in dashed contour). In *blue* a cross-section for detailed examination. P1, P2 and P3 are locations analysed in Soares et al. (2014), P4 location where a maximum future CLLJ occurrence anomaly is found, and P5 location where a maximum jet frequency of occurrence is found in the historical simulation

(Cardoso et al. 2013), solar irradiance (Magarreiro et al. 2016), and offshore wind in Soares et al. (2014). Moreover, its results were used to study the moisture recycling processes in Iberian (Rios-Entenza et al. 2014), and the diurnal cycle of the coastal clouds in western Iberia (Martins et al. 2015) both affected directly by the CLLJ dynamics. Other examples, are the studies focused on the development of wildfires propagation models and the characterization of the climatic cooling potential and energy savings for Iberia, using direct ventilation and evaporative cooling systems (Campaniço et al. 2016). All these studies showed the high quality of the results produced using WRF to describe the Iberian climate variables. Recently, the full set of simulations was also used for climate change assessment studies in Iberia, analysing the precipitation changes projected for a future climate (Soares et al. 2016). A more comprehensive description of the model set-up and parameterizations used can be found in Soares et al. (2012) and Cardoso et al. (2013). As in the hindcast, the WRF results are hourly.

The historical simulation is not synchronized and therefore only its statistics can be compared with observations. The future simulation follows the greenhouse gases emissions of the RCP8.5 scenario (Riahi et al. 2011). The RCP8.5 is one of three possible future scenarios and is named according to the equivalent effect, relative to pre-industrial era, of greenhouse gases concentrations in the radiative forcing values in the year 2100 (i.e. $+8.5$ W m^{-2}). The other proposed emission scenarios are RCP2.6 and RCP4.5. In the RCP 8.5 the global annual greenhouse emissions rise throughout the twenty-first century, while in RCP2.6 emissions peak between 2010 and 2020 and in the RCP4.5 emissions peak around 2040 and diminish afterwards (Moss et al. 2010; van Vuuren et al. 2011; Riahi et al. 2011). Although RCP8.5 is the more extreme option, the current emission record support it a plausible scenario.

2.2 Methods

The hourly vertical profiles of the zonal and meridional wind speed components and of the temperature allows the detection of CLLJ occurrences in the region of interest (Fig. 1b), following the algorithm proposed by Ranjha et al. (2013), and used in Soares et al. (2014), Semedo et al. (2016) and Cardoso et al. (2016). This algorithm seeks for wind speed maxima associated with a sharp temperature inversion within the MABL. Following, Ranjha et al. (2013), a CLLJ occurs when the following criteria are met: (1) the jet maximum height is below the first kilometre; (2) the wind speed at jet maximum increases by at least 20 % from the wind speed at the surface; (3) the wind speed above the jet maximum decreases to below 80 % of the wind speed at the surface (i.e. a 20 % falloff) in the first five kilometres; (4) the jet maximum occurs within a temperature inversion. These criteria were applied sequentially to hourly wind-speed and temperature vertical profiles to detect the location and frequency of CLLJ. Once identified as a CLLJ occurrence in a grid point, a number of statistics are computed to portray: the local hourly CLLJ frequency

of occurrence at different time scales (monthly to seasonal), the mean wind speed, the regional probability distribution functions (PDFs) of jet height of occurrence and jet speed and the jet and surface wind roses.

The referred detection algorithm is applied to the historical and future climate simulations, and their results are compared to assess the expected future changes on the properties of the Iberian CLLJ. But, first, a comparison focused in the CLLJ properties simulated in the historical run is performed against the ones of the hindcast simulation reported in Soares et al. (2014). These authors evaluated extensively the WRF wind and temperature results against observations, showing a very good model performance and its quality to simulate the CLLJs. Finally, in order to give extra weight to the quality of historical WRF results, a comparison of the historical vertical profiles (temperature and wind speed) with available radiosondes (only Lisbon and LaCoruña) was performed (Table S1 in supplemental material).

3 Results

3.1 Evaluation of the historical simulation

The maps of CLLJ frequency of occurrence results of the historical simulation, for winter (December to February—DJF), spring (March to May—MAM), summer (June to August—JJA) and autumn (September to November—SON) along the Iberian Peninsula coastal waters, can be seen in Fig. 2. The frequencies of occurrence are in close agreement with the ones of the hindcast simulation by Soares et al. (2014; their Fig. 6, see supplemental material, Figure S2). In both present climate simulations (hindcast and historical) summer presents the highest frequencies of CLLJ occurrence, with values over the full western Portuguese coast above 28 %, and local maxima around 32 % downwind of the three main capes along the western cost of Iberia (Finisterre, Roca, and São Vicente). The historical run produces a smaller frequency local maximum southwest of Cape São Vicente, in Portugal, which seems to be connected to the stronger and more persistent winds from Gibraltar. In spring the historical run shows considerable lower frequencies of occurrence than the hindcast, less than 5 % in large areas offshore Iberia; while in autumn the opposite happens, i.e. about more 2–3 % downwind of the main coastal capes. In winter both runs show the same kind of maximum values (bellow 8 % of frequency of occurrence), localized in small areas downwind the more conspicuous capes, like Cape Carvoeiro. Positive identifications of coastal jets off the Strait of Gibraltar are visible in summer and in the intermediate seasons (as in Soares et al. 2014), which correspond to a gap wind named Levante (Dorman et al. 1995). These southern coast winds are not studied here and will not be considered in the statistical analysis below; the area where occur it is masked and positive CLLJ occurrences are filtered out.

In Table 1 a summary of the main seasonal spatial CLLJ statistics for the historical run is presented. These include the mean, median and maximum values of: CLLJ frequency of occurrence, jet wind speed and jet height. Additionally, Table 1 shows a comparison of the historical and hindcast CLLJ statistics comprising: the spatial correlation of the seasonal CLLJ frequencies of occurrence and the differences between the mentioned jet properties. Values for the full domain (All) and for the north (BoxN) and south (BoxS) boxes, depicted in Fig. 1b, are shown in Table 1.

For summer, the spatial correlation of the CLLJ occurrences are high, 0.96 for the full area in analysis, 0.94 and 0.96, for the north and south domains (Fig. 1b), respectively. The correlations for winter and spring are also high, between 0.89 and 0.95. But, in autumn smaller spatial correlations are found, from 0.80 to 0.48. Regarding the mean and median values of the CLLJ frequency of occurrence, the differences between the control and the hindcast are rather small, ~1 % out of ~20 % for the full domain, for JJA. The larger differences are, again, found in spring, and are much smaller in autumn and winter.

In Fig. 3 the summer main statistical properties of the Iberian CLLJ result of the historical simulation are plotted. These include the jet height PDF, the jet wind speed PDF, the jet wind rose, the surface jet wind rose, a mean wind and potential temperature cross-section and a vertical wind and potential temperature cross section both when the jet occurs.

The comparison of Fig. 3 with Figure S2 (Fig. 7 from Soares et al. (2014)) reveals that the statistical features of the historical simulation are rather similar to the hindcast ones. The histograms of jet heights and of jet wind speed are almost identical (Fig. 3a, b), where the height median is around 290 m for both simulations, and the median jet speed in around 15 ms^{-1}, with only 3 % of relative difference between the two simulations. Likewise, the most persistent jet wind direction is north–north-easterly for more than 35 % of occurrences and north with values less than 25 % (Fig. 3c). The historical surface, wind when the jet occurs (Fig. 3d), shows a striking persistence above 40 % from north and around 25 % from NNE, and less than 15 % NNW. The potential temperature (contour lines) and wind speed (colours) cross section, when the jet occurs, of the historical simulation (Fig. 3e) is analogous to the one presented by Soares et al. (2014). The thermal structure of the lower atmosphere shows a well-mixed MABL capped by warmer air. This well mixed layer is under the jet structure which slopes towards the coast. The mean jet core is between 200 and 400 m heights and has wind speeds above

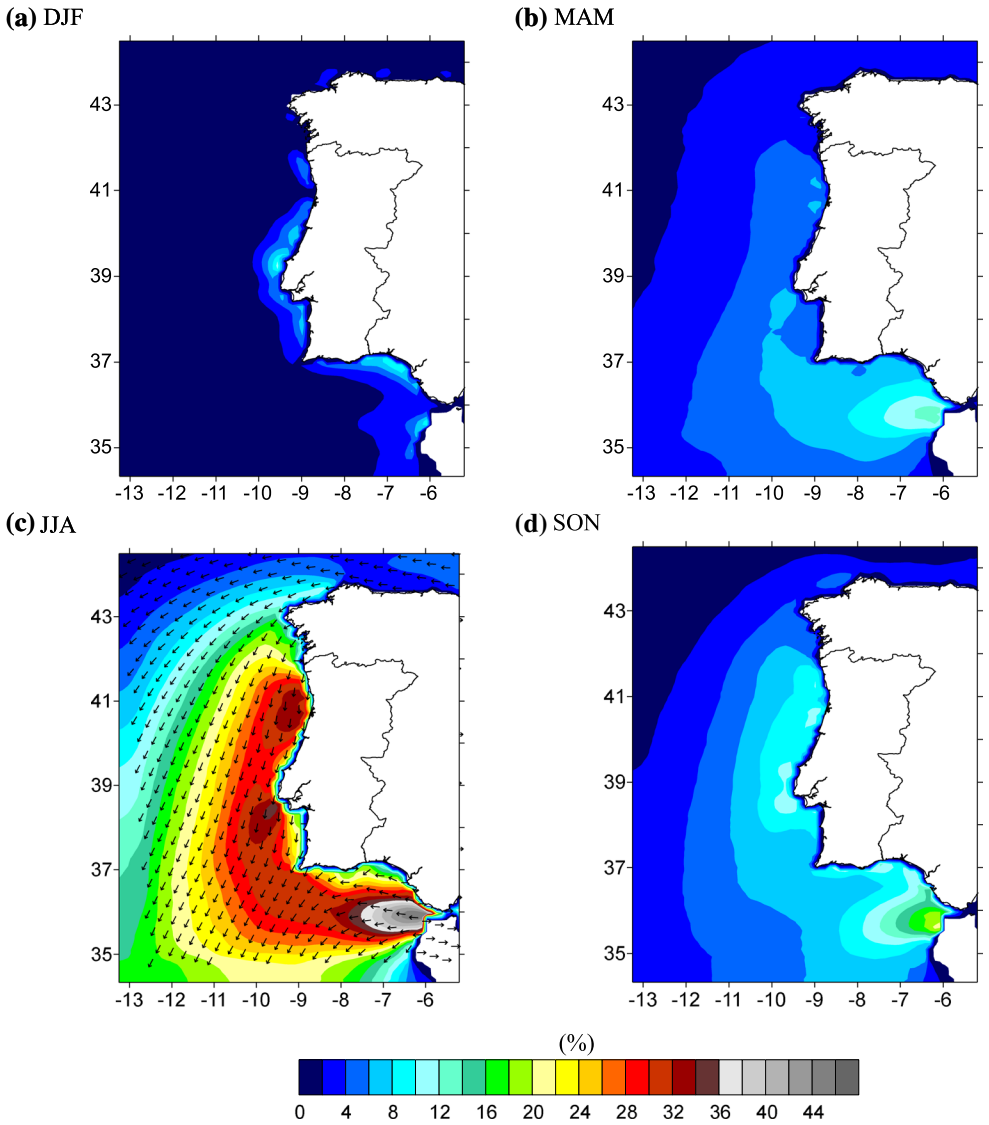

Fig. 2 Maps of hourly CLLJ frequency of occurrence (%) of the historical simulation for each season: **a** winter—DJF, **b** spring—MAM, **c** summer—JJA and **d** autumn—SON. The same colour scale as Soares et al. (2014) is used but added with *grey bars* for higher values to enhance differences

12 ms^{-1}. The potential temperature (contour lines) and vertical wind (colours) cross section, when the jet occurs, (Fig. 3f) shows the typical subsidence air over the ocean associated with the Azorean anticyclone. This prevalent subsidence air over the ocean is stronger above the jet eastern limit, which compresses the isentropes and enhances the horizontal wind speeds and by definition of the jet core is located where higher wind speeds are found. It is relevant to mention that the CLLJ vertical structure and wind intensity are highly dependent on the vertical resolution and on the planetary boundary layer scheme used (Bravo et al. 2008; Hu et al. 2010). As Bravo et al. (2008) pointed out a not very high vertical resolution may generate a weaker and too vertically wide low-level jet. Moreover, the setting of a relatively high value for the minimum TKE, as considered in the Mellor–Yamada–Janjic planetary boundary layer scheme, may exacerbate mixing and contribute as well to a too high and too weak LLJ.

Although in the historical simulation WRF is forced by a free running GCM (EC-EARTH) and not by a reanalysis (ERA-Interim), where offshore and onshore observations are assimilated, and two different time windows were covered (1971–2000 for the historical run and 1989–2007 for the hindcast) the historical results follow closely the ones for the hindcast (Soares et al. 2014). This resemblance is essential to increase the confidence in WRF results, in its ability to describe the present and future climate properties of the Western Iberian CLLJ, and on its suitability

Table 1 Statistical comparison between the hindcast and the historical coastal jet properties: spatial correlation of seasonal frequencies of occurrence, relative errors of mean and median of jet wind speed and jet height. Relative differences (Dif.) between the historical and the hindcast, in percentage (historical–hindcast)/hindcast for all variables except for frequencies of occurrence (historical–hindcast) and for spatial correlation coefficients

		DJF		MAM		JJA		SON	
Properties	Domain	Dif.(%)	Control	Dif.(%)	Control	Dif.(%)	Control	Dif.(%)	Control
CLLJ frequency of occurrence									
Spatial correlation	All	–	0.90	–	0.91	–	0.96	–	0.80
	BoxN	–	0.89	–	0.93	–	0.94	–	0.77
	BoxS	–	0.90	–	0.95	–	0.96	–	0.48
Mean (%)	All	−0.08	2.27	−3.45	5.31	−0.38	20.59	1.2	7.10
	BoxN	−0.03	2.51	−4.90	4.94	−1.62	22.26	1.32	8.07
	BoxS	0.00	2.89	−3.57	6.04	1.42	27.40	1.48	8.73
Median (%)	All	−0.11	1.08	−3.61	3.61	−1.21	18.95	0.54	4.30
	BoxN	−0.28	1.21	−5.41	3.33	−2.91	20.42	1.08	5.11
	BoxS	0.00	1.61	−4.18	4.57	1.48	26.61	1.21	6.45
Max (%)	All	−8.00	25.30	5.78	57.53	14.92	87.77	7.92	51.39
	BoxN	−7.50	25.30	6.05	47.58	14.92	87.77	7.92	51.39
	BoxS	−8.46	24.87	0.27	45.30	16.04	81.18	16.25	49.86
Jet wind speed (m/s)									
Mean	All	8.36	11.93	0.08	13.34	2.79	14.76	1.45	11.86
	BoxN	7.18	11.49	−4.73	12.48	−1.81	14.62	−2.87	11.18
	BoxS	9.30	12.10	−0.15	12.90	3.41	14.55	5.41	11.70
Median	All	6.84	11.24	−1.00	12.82	3.40	14.61	1.24	11.41
	BoxN	7.07	11.06	−5.56	12.07	−1.89	14.50	−3.50	10.75
	BoxS	5.26	11.01	−2.06	12.39	4.17	14.49	4.44	11.28
Max	All	3.92	32.10	9.38	36.03	21.62	40.22	9.59	32.69
	BoxN	4.49	32.10	7.40	33.97	14.18	35.76	−1.58	28.09
	BoxS	11.59	31.58	6.77	33.73	31.71	38.59	10.75	31.41
Jet height (m)									
Mean	All	−3.40	244.12	−4.82	264.58	−4.49	302.13	−2.94	252.52
	BoxN	−1.54	204.90	−7.04	214.97	−11.29	244.98	−8.94	202.59
	BoxS	−1.60	236.83	−8.70	253.89	−6.79	293.95	−1.10	242.63
Median	All	−1.58	227.93	−17.68	234.31	−1.00	290.92	−0.80	236.04
	BoxN	−0.56	180.20	−20.45	183.49	−18.51	234.32	−2.12	184.34
	BoxS	−1.62	224.64	−18.62	232.63	−1.53	290.22	−0.64	235.13

to disclose the climate change signal on the coastal jet features.

3.2 Future projections for the Iberian CLLJ

According to the WRF simulation following the RCP8.5 future scenario, the overall values and the spatial pattern of future frequencies of occurrence of the Iberian CLLJ show considerable changes for the end of the twenty-first century. The maps of the projected seasonal CLLJ frequency of occurrence for the end of this century, as well as the seasonal coastal jets frequency of occurrence anomalies (future minus present) are shown in Fig. 4. A Student's *t* statistical significance test was applied to the spatial distributions, and the results show that the differences between future and historical simulations are statistically significant. Additionally, in Table 2 a summary of the main coastal jet future properties and correspondent changes, comparing the historical and the future simulation, are listed.

Future CLLJ climate (Fig. 4a–d) reveals significant occurrences along almost the full extent of the western Iberian coast, with frequencies above: 36 % in the summer (values in grey), 10 % in the spring and 12 % in autumn. These 3 seasons show maximum values of 46, 14 and 16 %, respectively, which are mainly localized in the northern half of the western coast.

For summer, the amplification on the persistence of the CLLJ is most notable. In the northern sector, the frequency of occurrence anomaly (future minus present) has a maximum around 18 %, which corresponds to almost doubling its presence in this region. An increase in the frequency of occurrence of above 10 % extends over the full western Iberian coast (Fig. 4; Table 2), pointing to not only a more persistent CLLJ but also to an enlargement of its region of

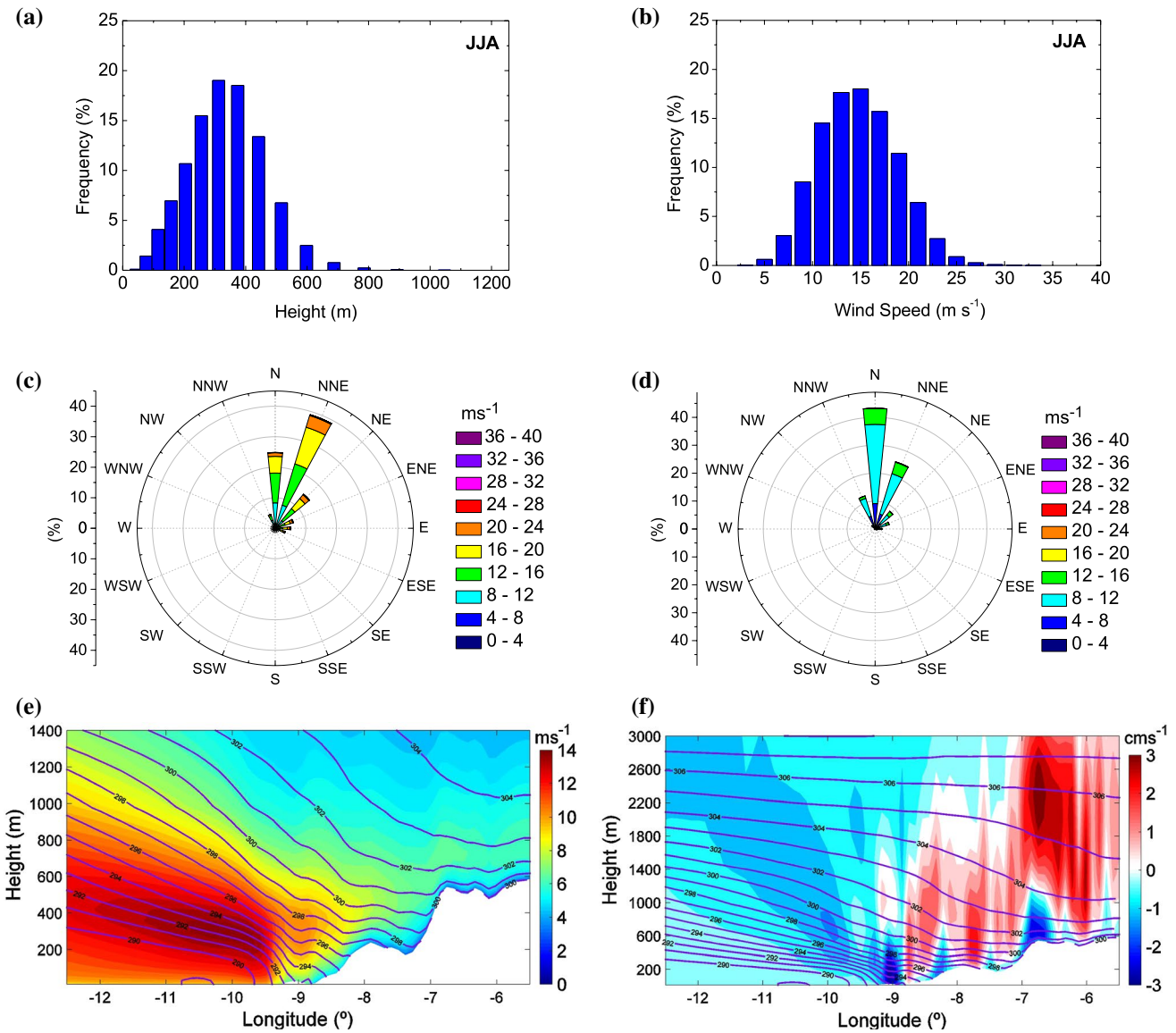

Fig. 3 Summer CLLJ statistics for Historical (1971–2000): **a** jet height histogram, **b** jet wind speed histogram, **c** jet wind rose and **d** jet surface wind rose and East–west cross-section at 38.41°, marked in *blue* in Fig. 1, where the *blue lines* are potential temperature and colours are **e** wind speed and **f** vertical velocity, both averages when the jet occurs

influence, especially in higher latitudes, in agreement with the results of Wang et al. (2015) and Semedo et al. (2016). The northern area where larger increases are expected, ~15 % on average in the BoxN (Table 2) are in agreement with the regions that in present climate revealed higher temporal variability (Soares et al. 2014). The consistency of the augment of persistence of summer coastal jets can also be observed in Fig. 5a, where boxplots of the full seasonal distributions of frequency of jet occurrence, for the selected areas in Fig. 1b, for present and future climates, are presented. In fact, there is a clear distribution shift for much higher values in the full area and in both sub-domains, which is stronger in the BoxN. For summer, in all areas, the present climate median frequencies are surpassed by future 25th percentile frequencies, and for the BoxN the present climate 75th percentile has similar values to the future 25th percentile, stressing the major changes projected for the future Iberian jet.

In Fig. 5b, c, the seasonal boxplots of jet wind speed and jet height, for present and future climates, are also plotted. For summer, the jet wind speed boxplots show a shift for higher jet speeds in the full area, in spite of some reduction in the southern sub-area (BoxS), which is compensated by a stronger increase in the northern sub-area (BoxN). In fact, the jet speed mean value increases around 2, 6 % and diminishes 2 %, respectively, for the full area, the north and

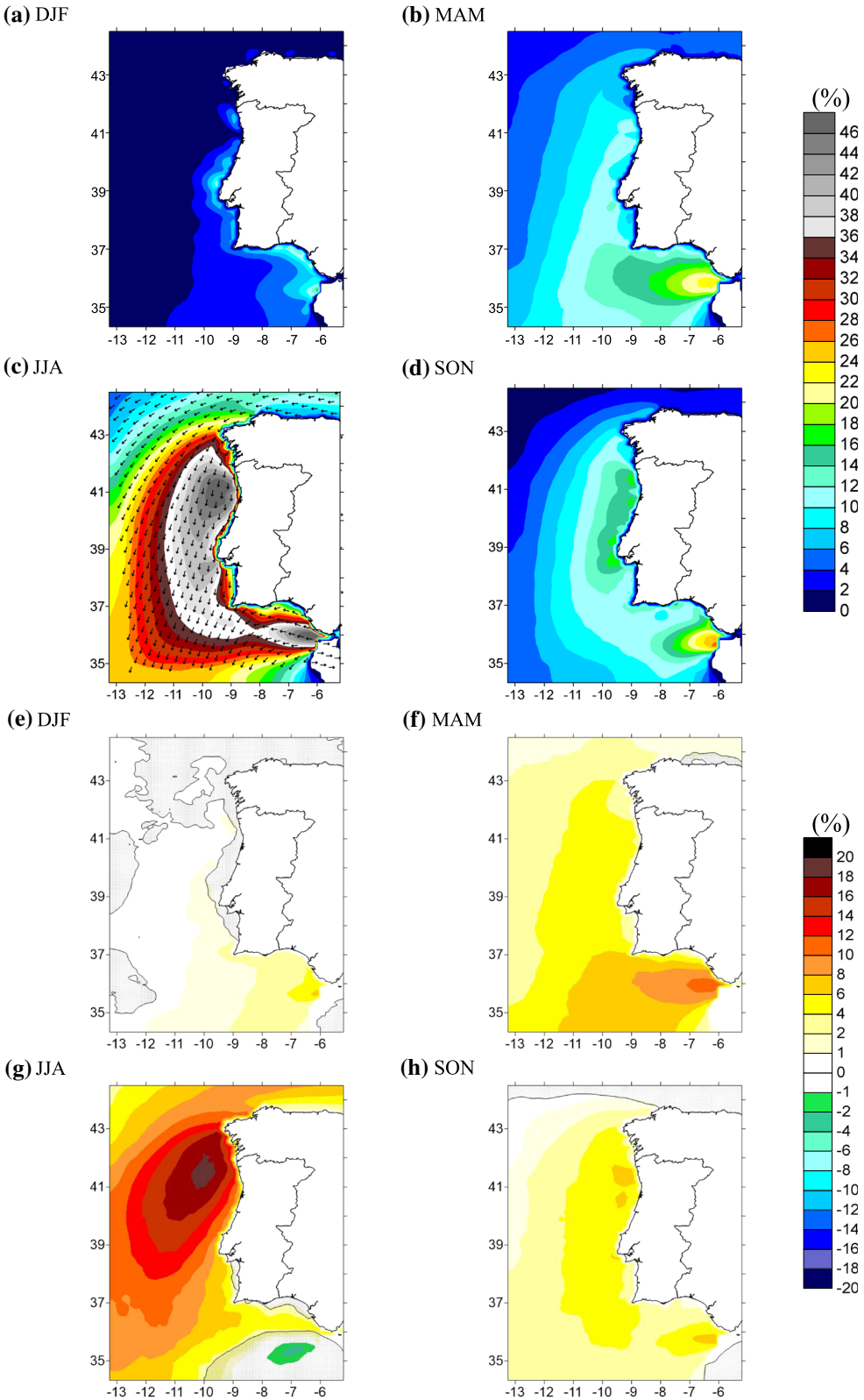

Fig. 4 Maps of seasonal hourly CLLJ frequency of occurrence (%) for future climate, for **a** DJF, **b** MAM, **c** JJA and **d** SON; the same colour scale as Soares et al. (2014) but added with *grey bars* for higher values. Maps of the differences (Future minus Historical) of seasonal hourly CLLJ frequency of occurrence (%) (2071–2100 minus 1971–2000), for **e** DJF, **f** MAM, **g** JJA and **h** SON. Shaded areas specify not statistically significant changes using a Student's *t* test at the 90 % confidence level

south boxes (Table 2). Overall, there is a reduction of values ranging between 5 and 17 ms^{-1}, and increasing occurrences of enhanced speeds from 17 to 27 ms^{-1}.

Similarly, the jet height boxplots (Fig. 5c) for summer exhibits a shift towards higher levels in a future climate in the full area, and strongly in the northern sub-area. This

Table 2 Summary of the jet properties changes projected for the end of the twenty-first century. Future values and relative differences (Dif.) to the historical results, in percentage (future–historical)/historical for all variables except for frequencies of occurrence (future–historical)

Properties	Domain	DJF		MAM		JJA		SON	
		Dif.(%)	Future	Dif.(%)	Future	Dif.(%)	Future	Dif.(%)	Future
CLLJ frequency of occurrence (%)									
Mean (%)	All	0.81	3.08	4.18	9.49	10.15	30.74	2.91	10.01
	BoxN	0.50	3.01	4.01	8.95	15.08	37.34	4.06	12.13
	BoxS	0.95	3.84	4.32	10.36	9.88	37.28	4.11	12.84
Median (%)	All	0.41	1.49	3.24	6.85	10.22	29.17	1.95	6.25
	BoxN	0.40	1.61	3.34	6.67	15.55	35.97	3.49	8.60
	BoxS	0.62	2.23	3.76	8.33	8.87	35.48	2.58	9.03
Max (%)	All	18.79	44.09	−2.42	55.11	3.22	90.99	16.67	68.06
	BoxN	18.79	44.09	7.26	54.84	3.22	90.99	8.05	59.44
	BoxS	18.95	43.82	8.33	53.63	−1.34	79.84	18.20	68.06
Jet wind speed (m/s)									
Mean	All	−1.93	11.70	2.55	13.68	1.90	15.04	2.70	12.18
	BoxN	−5.66	10.84	0.80	12.58	5.61	15.44	7.33	12.00
	BoxS	−0.74	12.01	1.32	13.07	−2.13	14.24	0.09	11.71
Median	All	−0.62	11.17	3.20	13.23	1.78	14.87	2.98	11.75
	BoxN	−6.33	10.36	0.66	12.15	6.55	15.45	7.44	11.55
	BoxS	2.36	11.27	2.26	12.67	−2.35	14.15	0.09	11.29
Max	All	9.91	35.28	7.30	38.66	−5.69	37.93	14.01	37.27
	BoxN	−4.11	30.78	−9.36	37.15	−0.50	35.58	3.60	29.10
	BoxS	0.63	31.78	11.56	37.63	−4.35	36.91	−0.67	31.20
Jet height (m)									
Mean	All	8.09	263.86	4.63	276.82	4.93	317.03	4.22	263.18
	BoxN	2.14	209.29	3.50	222.49	6.27	260.33	5.72	214.17
	BoxS	9.54	259.43	4.23	264.63	4.55	307.31	4.71	254.05
Median	All	2.46	233.53	21.23	284.05	1.41	295.02	1.35	239.23
	BoxN	1.04	182.08	2.62	188.30	1.46	237.73	1.46	187.03
	BoxS	3.04	231.47	1.36	235.80	1.21	293.73	1.21	237.98

shift is accompanied for an enlargement of the distributions, which doesn't alter substantially neither the mean nor the median values of the jet height. The southern sub-area only shows a small widening of the distribution. The changes of jet wind-speed and jet height were tested for their statistical significance, through a Kolmogorov–Smirnov test, and all the changes are statistically significant at a 95 % confidence level.

Looking at some other future properties of the summer coastal jets, Fig. 6 displays the future CLLJ wind rose, the surface wind rose when the jet occurs and the mean cross sections of potential temperature and jet speed and vertical velocity. The projected jet direction change points out to an increased northerly frequency (Fig. 6a) resulting from a reduced NNE jet wind direction when compared to present climate (Fig. 3c). Accordingly, at the surface, the wind, when the jet occurs, shifts from NNE to N, and the highest frequencies remain from the northern sector (Fig. 6b). The jet height-speed histograms (not shown) for present and future are similar, but accordingly, with the two previous PDFs, revealing a common frequency change for the occurrence of the jet at higher vertical levels and with superior speeds. Finally, Fig. 6c–d presents cross sections for the potential temperature and wind speed, and potential temperature and vertical velocity, averages when the jet occurs (in blue in Fig. 1b). It can be seen a general warming that corresponds roughly to 2 K in the MABL and 4 K aloft. For both present and future climate, the jet within the MABL is easy to identify, but with greater speeds and larger spatial coverage in the future scenario. The CLLJ slopes upward offshore, accompanying the MABL inversion slope.

The MBL sloping downward toward the coast is associated with the cross-shore pressure gradient, which maintains a near geostrophic equilibrium with the Coriolis deflection of the jet (Garreaud and Muñoz 2005). This upward slope offshore is due to the increasing sea-surface temperatures offshore, the weakening to the west of the synoptic-scale subsidence (Fig. 6d) and the enhanced subsidence closer to the coast due to the daytime regional subsidence associated to the return flow of warm air from land to sea (Beardsley

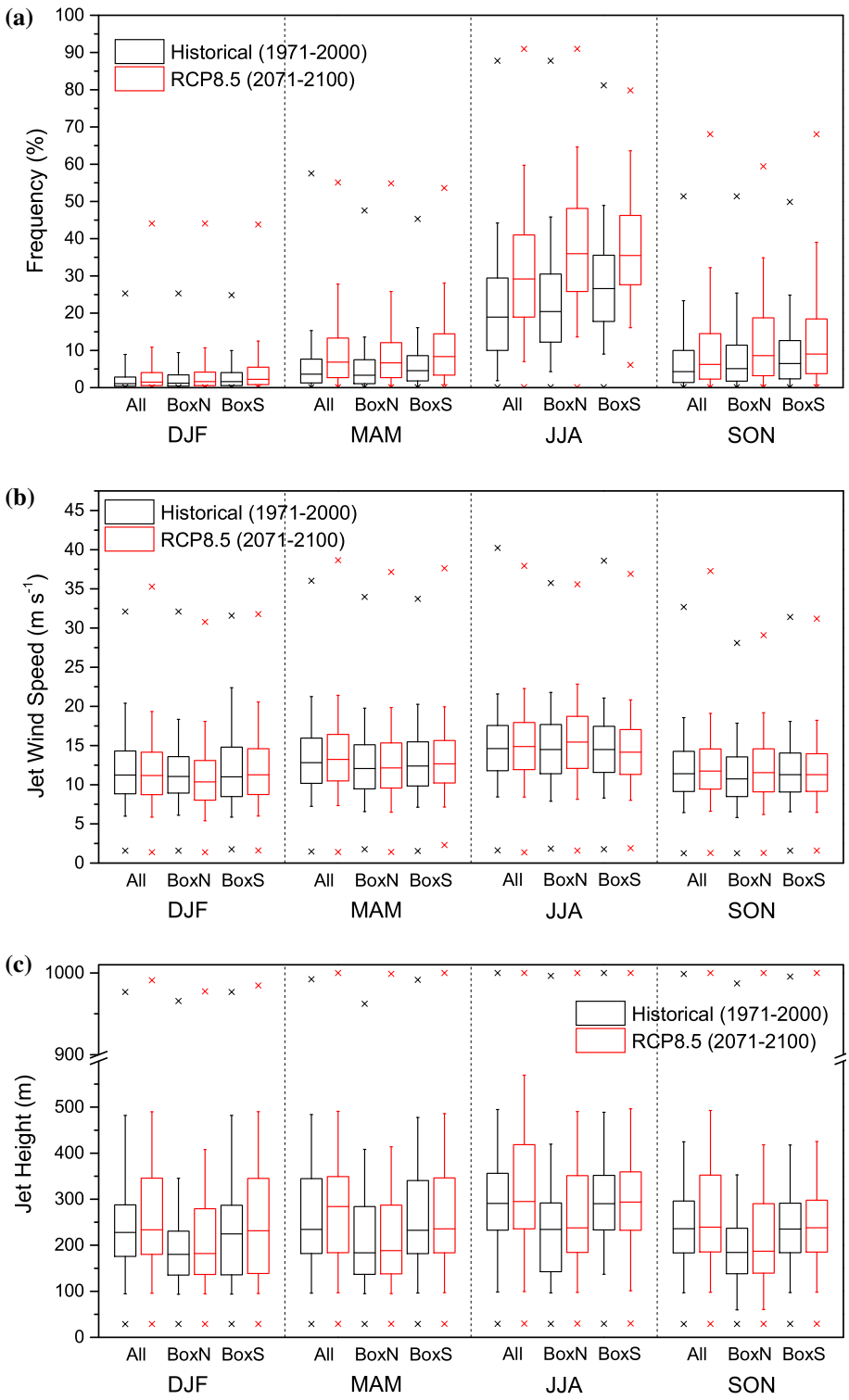

Fig. 5 Boxplots of the CLLJ results for the historical (*black*) and the future projections (*red*), for the different regions of Fig. 1b, for all seasons, for **a** jet frequency of occurrence, **b** jet wind speed, and **c** jet height. Individual boxes span from the 25th to the 75th percentile, with the median represented by a *straight line*, with the absolute maximum and minimum indicated by *crosses*

et al. 1987). The CLLJ maintains a semi-geostrophic balance, in which the background pressure gradient plus the induced mesoscale pressure perturbation are balanced by turbulent and acceleration terms (Cui et al. 1998).

The future anomalies of the large-scale subsidence, the synoptic pattern flow and the thermal contrast between land–ocean, may contribute to the understanding of some of the mechanisms responsible for the CLLJ changes. It is important to refer that CLLJs are not in geostrophic balance but are deeply rooted in the synoptic large and regional scale flows. Moreover, the momentum turbulence role should not be forgotten in a more detailed view, which

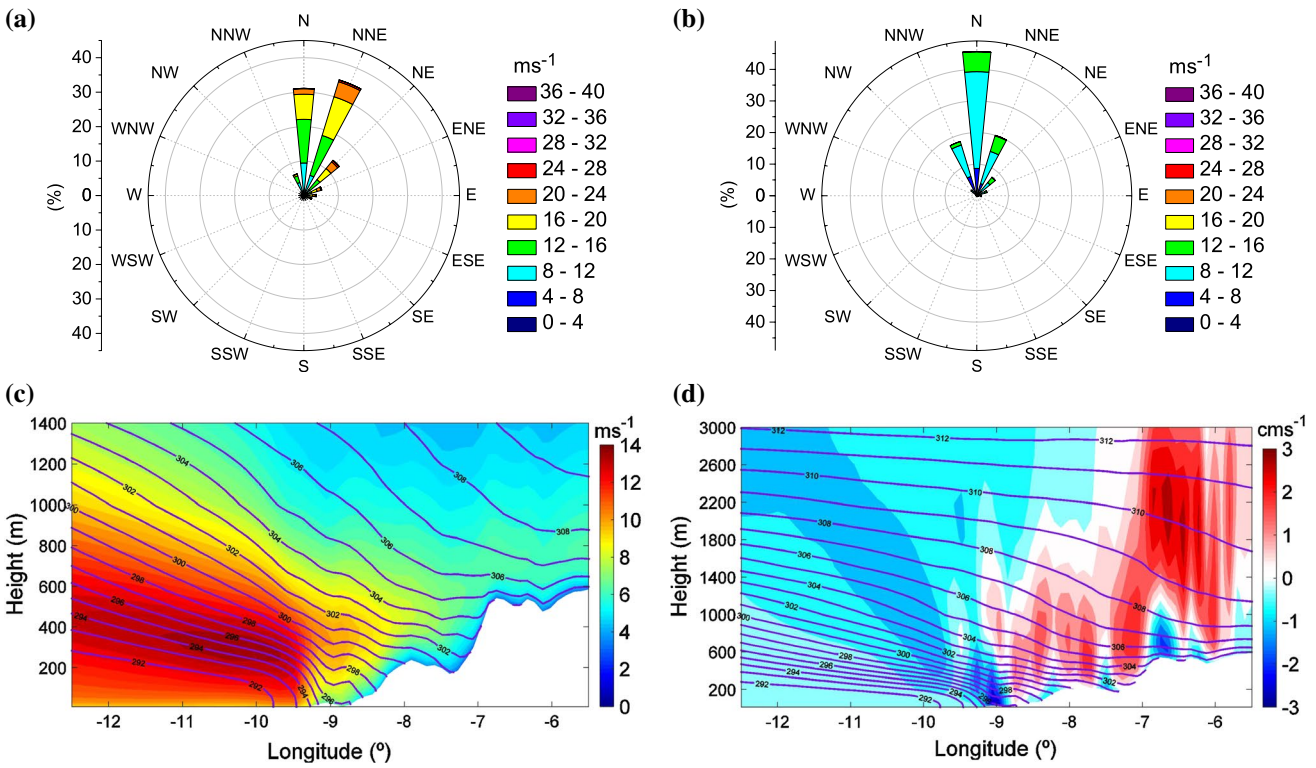

Fig. 6 Summer CLLJ statistics for future simulation (2071–2100): **a** jet wind rose, **b** Jet surface wind rose and East–west cross-section at 38.41°, marked in *blue* in Fig. 1b, where the *blue lines* are potential temperature and colours are **c** wind speed and **d** vertical velocity, both averages when the jet occurs

is out of the reach of the current study, based on a long climate simulation.

The inspection of present and future vertical velocity cross-sections (Figs. 3d, 6d) does not reveal any significant change on the large-scale subsidence. Figure 7 presents the future mean sea level pressure (mslp) and the correspondent geostrophic wind results for EC-EARTH, and their respective anomalies (future compared to present). The mslp shows a positive anomaly in the north sector, centred in the British Islands, revealing a north-easterly broadening and larger persistency of the Azorean anticyclone, and consequently a larger influence over north Iberia. Simultaneously, a negative anomaly coexists in inland Iberian, which corresponds to an intensification of the thermal low over land. This synoptic pattern has an intense correspondent signal on the geostrophic wind, which amplifies over 4 ms^{-1} offshore the northwest of Iberia, where the higher increases of the coastal jet occur.

The annual cycle of surface temperature land–ocean differences, for the historical (1971–2000) and the future (2071–2100) simulations, for the marked boxes of Fig. 1b, is plotted in Fig. 8. In the boxes, concerning ocean or land temperatures, only ocean or land grid-points are taken in account, respectively. The surface temperature differences between land and ocean expose increasing values in future climate throughout the full annual cycle, but higher in summer, and larger in the north regions. Subsequently, it is clear that the two main CLLJ forcing ingredients, the Anticyclone-Thermal Low dipole and the land–ocean thermal contrast, appear enhanced in future climate, and especially in the north half of western Iberia. All this, adds to an increase of the CLLJ persistency. Obviously, the important feedbacks between the CLLJ and upwelling are not represented in these simulations, since sea surface temperature is updated according to the forcing data. An ocean–atmosphere coupled simulation would be very important to analyse these feedbacks in a future climate, but is out of the scope of the current study.

In the intermediate seasons, the jet frequencies of occurrence anomalies, between future and historical simulations (Fig. 4f, h; future minus present), reveal a small intensification of occurrences, on average around 4 % (Table 2), extending offshore over 300 km, in spring, and more than 200 km, in autumn. The seasonal boxplots of the jet frequency (Fig. 5a) show, for both intermediate seasons, a distribution shift for a larger persistence of coastal jets, but with less expression than in summer. Moreover, a stronger anomaly in the extreme values frequencies can

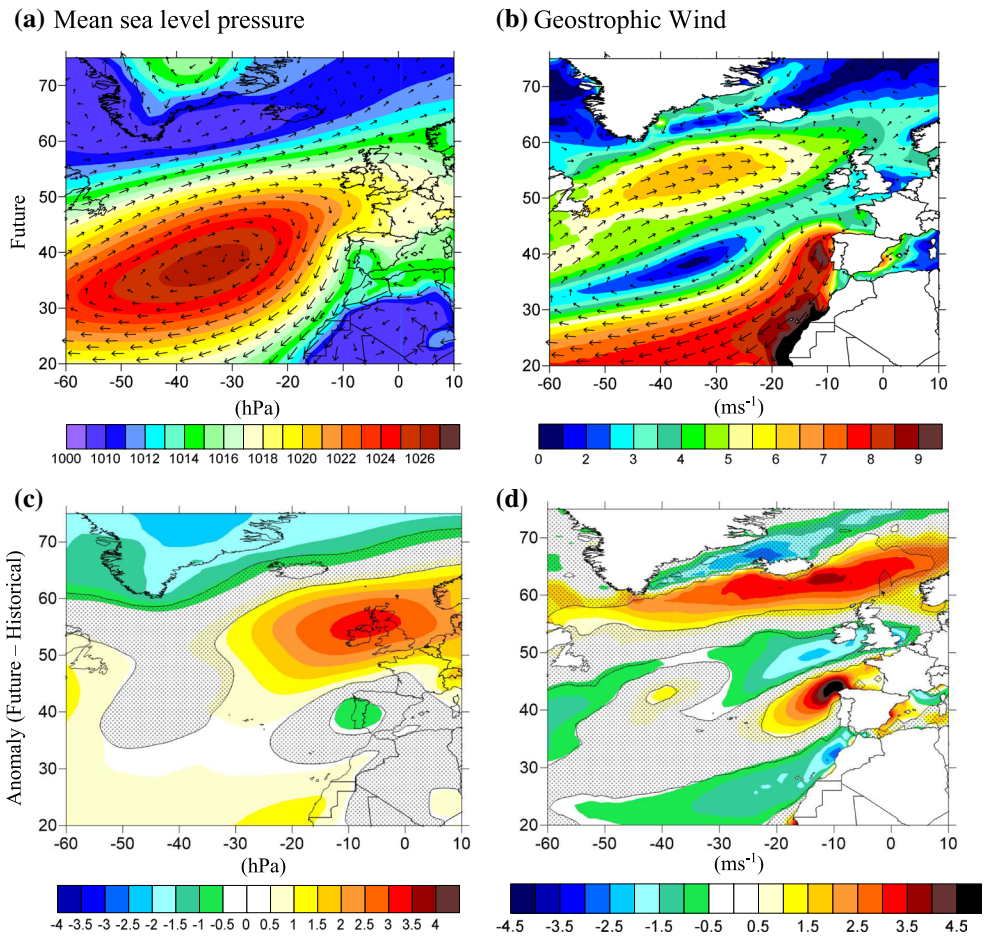

Fig. 7 Summer mean sea level pressure and correspondent geostrophic wind results of the EC-EARTH model future run (2071–2100) and anomalies against the historical simulation (1971–2000). *Shaded areas* specify changes not statistically significant using a Student's *t* test at the 90 % confidence level

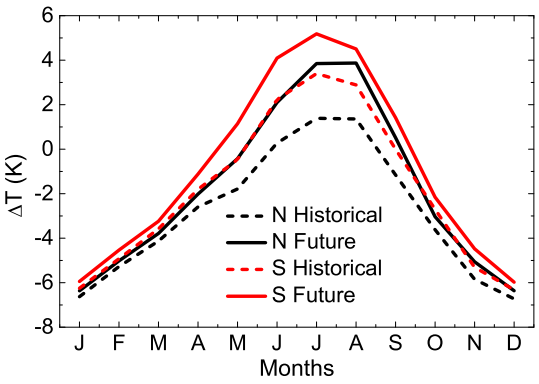

Fig. 8 Annual cycle of land–ocean differences of surface temperature (2 m) for the *marked boxes* in Fig. 1b, for the Historical (1971–2000) and the Future (2071–2100) simulations, future minus historical

be identified, for both the southern and the northern boxes, with maximum values increasing over 8 %, and in particular, in autumn in the southern region an 18 % growth is found (Fig. 5a; Table 2). The plots regarding the projected changes of the jet properties for the intermediate seasons (Figs. 5, 9; Table 2) highlight the common trend to the summer, but with smaller magnitude. The shift for higher jet wind speeds is clear in Fig. 5b, where future spring and autumn are expected to have an increase in the frequencies of greater jet wind intensities, when compared to the historical period. This augment is larger in autumn, in the northern area (BoxN), where the jet mean speed is expected to rise over 7 %. Concerning the jet heights (Fig. 5c), in future spring and autumn a modification for higher altitudes for jet occurrence is also expected. In fact, for both seasons, the boxplots reveal wider distributions and increases in all medians and mean values. In what regards to the jet wind direction, the projected changes are less noticeable than in JJA. In spring, the historical and future jet wind roses are almost identical, where, in both cases, the most persistence jet direction is from NNE, with frequencies of occurrence of about 25 %, and the other directions are almost completely comprised in the full NE-N quadrant (Fig. 9a, b).

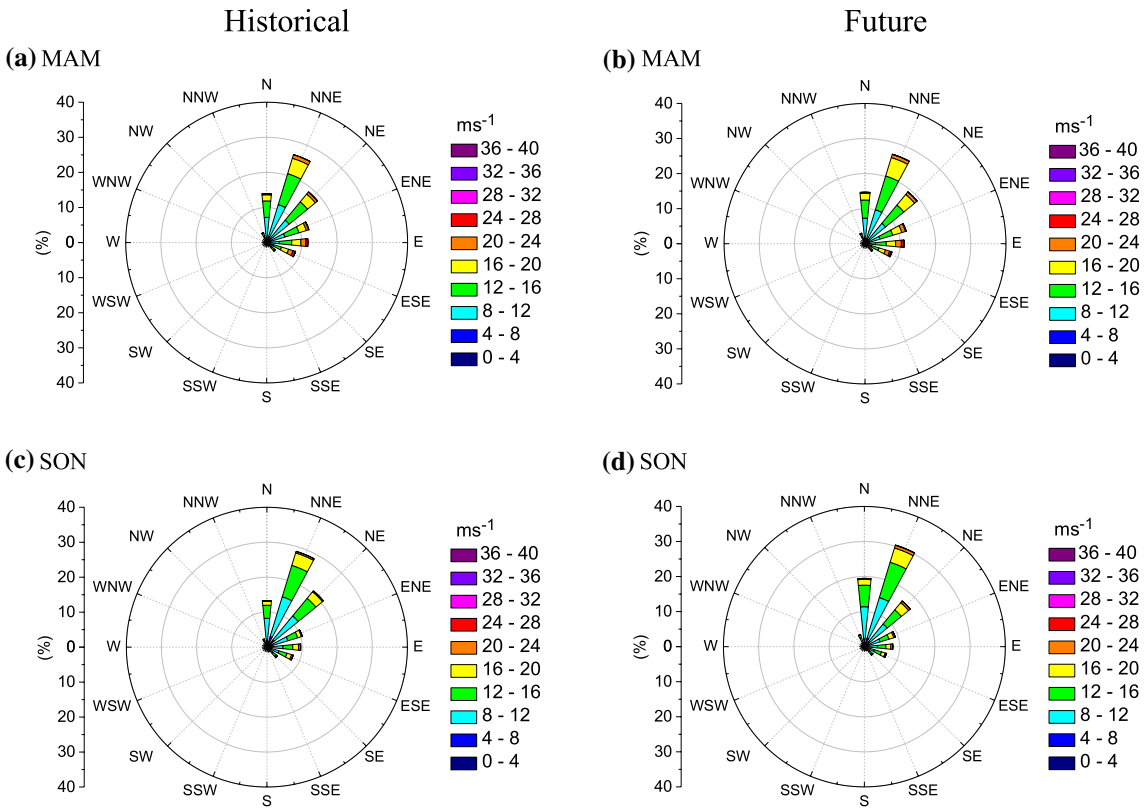

Fig. 9 CLLJ statistics for historical (1971–2000) and future (2071–2100) simulations: **a**, **b** jet wind rose for the historical and future simulations both for MAM, and **c**, **d** Jet wind rose for the historical and future simulations both for SON

For autumn, in agreement with the Fig. 4, where a more expressive increase of jets is projected for autumn than in spring, also here a partial shift to northerly wind appears, like in summer.

The CLLJ season seems also to temporally enlarge its influence in future climate. For the contiguous months to JJA, May and September, the frequency of jet occurrences grow significantly, around 10 % along all the coast extension, almost doubling its influence in these months (Figs. 10, 11). The summer months that experience a greater increase of frequencies of occurrence are June and July, reaching absolute values of around 50 % (Fig. 10), but enlarging its spatial influence, covering the full western offshore region of Iberia. Still it can be seen that for the full annual cycle the CLLJ occurrences grow, roughly 5 % in March, April, October and November, with the exception of the winter months (DJF). In general, the variability of the CLLJ frequency also increases spatially and temporally, with increased values of standard deviation further away from the shore, and with the exception of August where a decrease is found (not shown). This weakening of the standard deviation shows August as the month when the CLLJ possess steadier prevalence.

To further illustrate the local changes in the CLLJs, the monthly frequencies of occurrence and mean jet wind speeds are plotted in Fig. 12, for 5 selected locations (Fig. 1b). The first three positions (P1, P2 and P3) are the points where Soares et al. (2014) identified the highest CLLJ frequencies of occurrence in the hindcast simulation. P4 is located where the maximum future anomaly is found, and P5 is the site where a maximum jet frequency of occurrence is found in the historical simulation. For all the sites a temporal enlargement of the CLLJ season is detected, for earlier and later than JJA. It is visible that local frequencies of occurrence over 20 % occur from May to October. In 4 out 5 locations the maximum frequency is anticipated one month, from August to July, in future climate. All the locations present frequencies of occurrence higher than 10 % from April to October in future projections, anticipating 1 month the CLLJ season and delaying also 1 month it's ending. The southern point (P3) is the one showing the lower increase in the CLLJ frequency of occurrence (~4 %

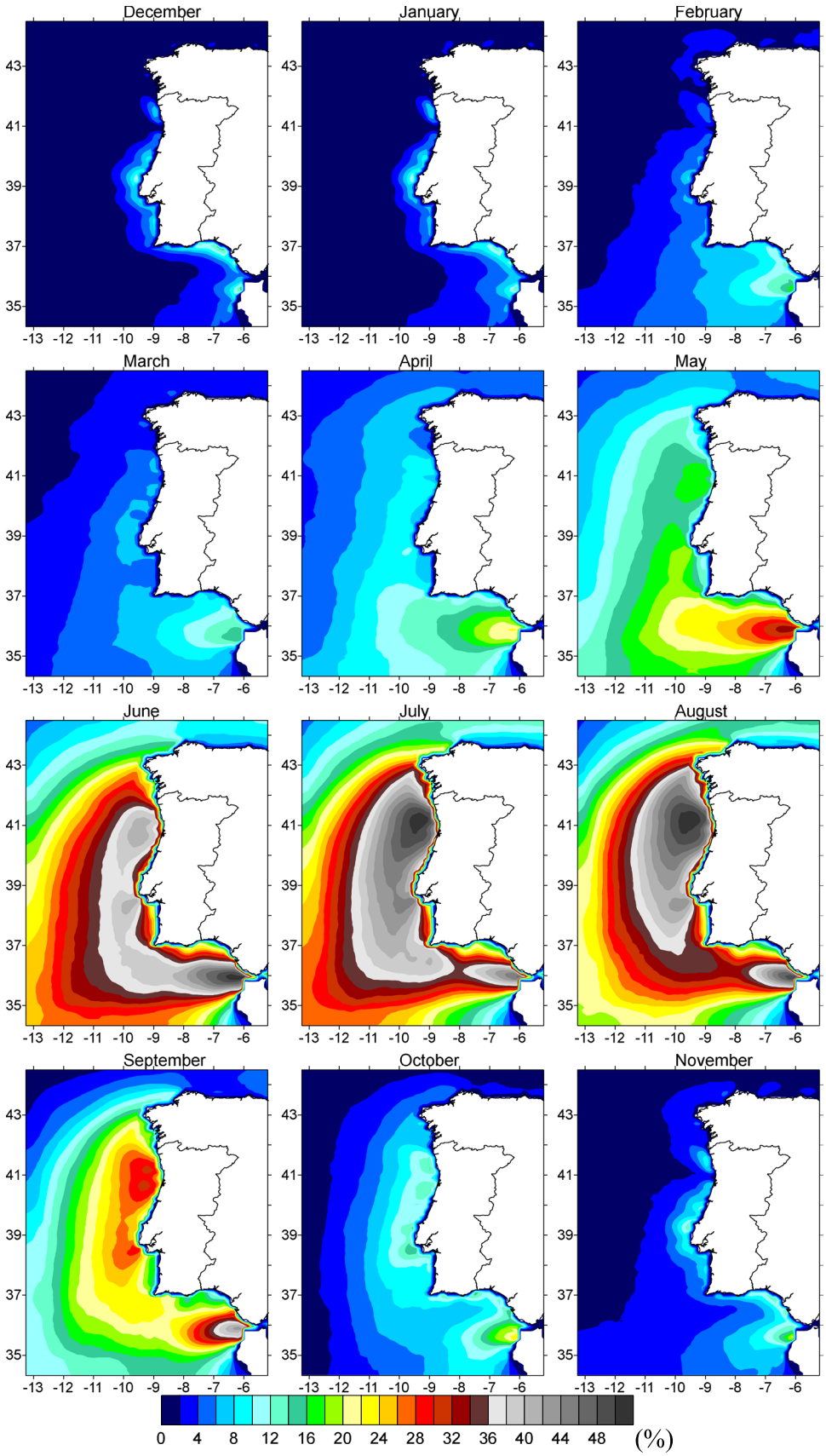

Fig. 10 Maps of monthly means of the hourly frequency of CLLJ occurrence (%) for future simulation 2071–2100. The same colour scale as Soares et al. (2014) but added with *grey bars* for higher values

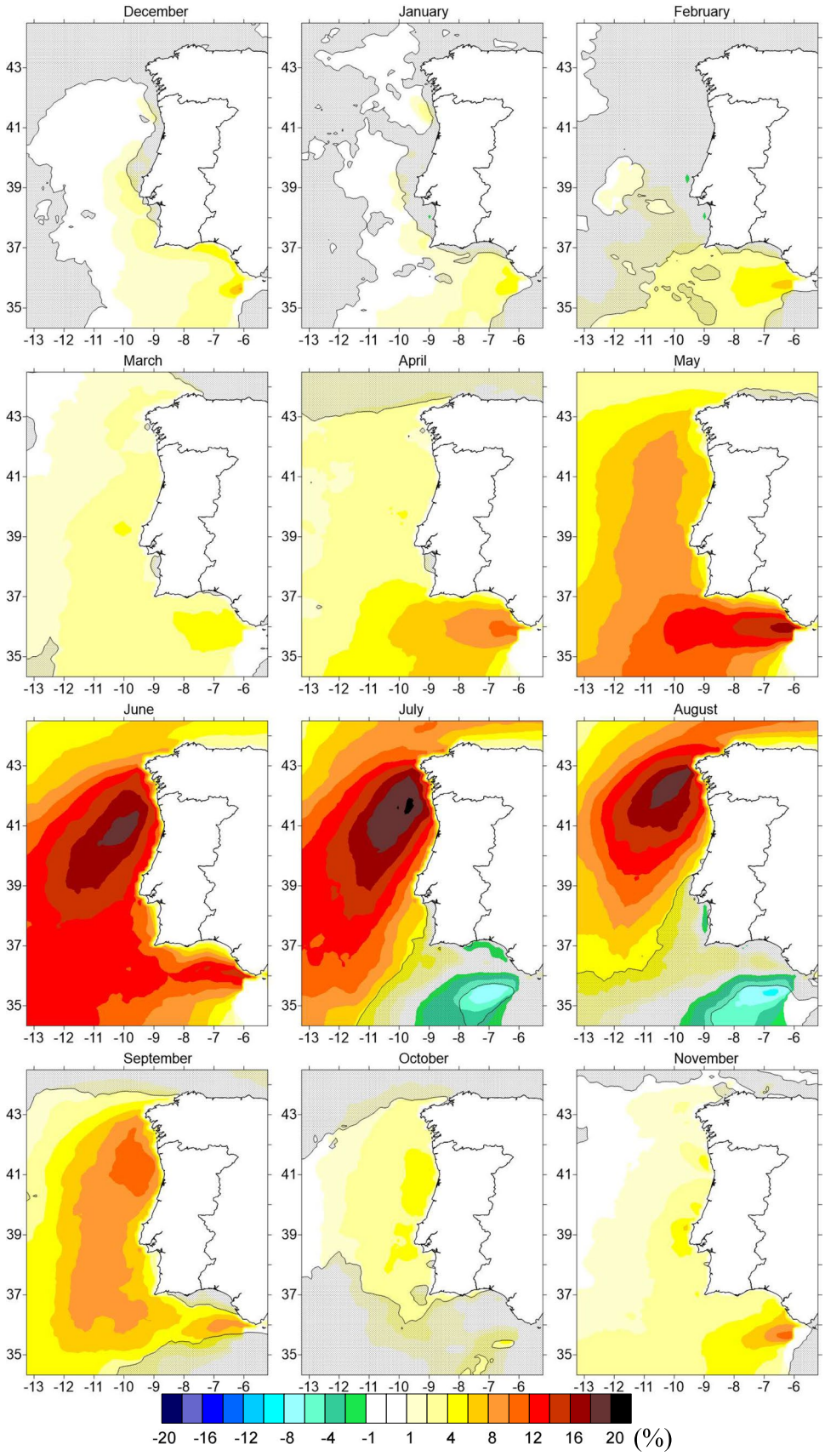

Fig. 11 Maps of differences of the monthly means of the hourly frequencies of CLLJ occurrence (%). Future minus Historical simulations (2071–2100 minus 1971–2000). *Shaded areas* specify changes not statistically significant using a Student's *t* test at the 90 % confidence level

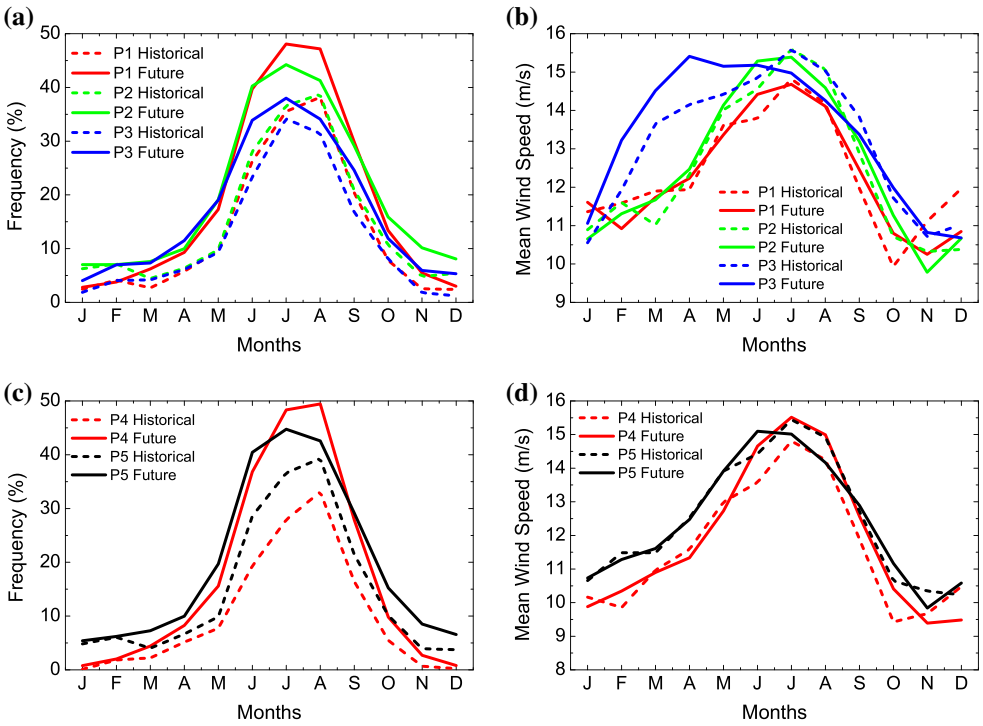

Fig. 12 Local mean monthly of **a–c** CLLJ frequency of occurrence (%) and **b–d** jet wind speed (m/s). P1, P2 and P3 are locations analysed in Soares et al. (2014), P4 location where a maximum future anomaly is found, and P5 location where a maximum jet frequency of occurrence is found in the historical simulation

in July) The northern points have much larger projected increases, which in the extreme case of P4 reaches approximately 18 %. Regarding, the jet wind speed annual cycle most of the locations present an increase of the jet mean wind speed, less than 1 ms^{-1}, that corresponds to an anticipation and delay of the CLLJ season.

4 Conclusions

The EBCS regions are amongst the most productive ocean ecosystems, where the atmosphere–land–ocean feedbacks play a key role in defining the regional climate (Bakun et al. 2015; Wang et al. 2015). In the EBCS regions, one can find some of the most arid regions of the world, namely, in the Mojave, Namibe, and Atacama deserts, and a crucial component is the presence of coastal jets (Nicholson 2010). Ranjha et al. (2013) using the ERA-interim reanalysis characterized the main CLLJs properties globally, and were the first to quantify the persistency of the Western Iberian coastal jet, reporting frequencies of occurrence above 20 %. Semedo et al. (2016), by means of a set of global climate simulations, identified robust and clear changes of the CLLJs properties in response to future warming, namely for the Iberia and the Oman CLLJs. This study projected future rise of CLLJ occurrences, in particular during summer, but also in the intermediate seasons, enlarging the duration of the CLLJ season, and an increase of the jet wind speeds. Recently, the western Iberian present climate CLLJ properties, were extensively described by Soares et al. (2014) using a high resolution regional climate simulation with WRF forced by ERA-Interim, where a maximum frequency of occurrence in summer above 30 % was found, with mean jet wind speeds around 15 ms^{-1} and a jet core located between 300 and 400 m heights.

In this study, the first climate change assessment study using a high resolution (9 km) regional climate simulation, focused in the Western Iberian CLLJ, is presented. Two simulations with the WRF model were analysed, one historical for the period 1971–2000, and another for future climate (2017–2100), in agreement with the RCP8.5 scenario, both forced by the EC-EARTH model. The CLLJ properties were computed for these two runs and compared to investigate their changes in the context of global warming. However, firstly a comparison of the CLLJ properties result of the historical simulation with the ones of the hindcast run presented by Soares et al. (2014), was performed. This comparison clearly demonstrates the similarity between these simulations regarding the western Iberian costal jet. The comparative analysis between future and historical simulations suggest significant modifications for the Western Iberian CLLJ. The hourly frequency of occurrence of the CLLJ increases in the full Western Iberian coast, from values of around 35 % to almost 50 % in summer. The relative increases of the frequency of occurrence are stronger in the north sector of Western Iberia, where the frequency of occurrence nearly doubles. The occurrence of coastal jets is expected to cover larger areas, both latitudinal and longitudinal. The CLLJ season is projected to be enlarged,

extending to more months of the annual cycle, only the winter months continue to have negligible occurrences. There is a shift for higher jet wind speeds and for the jet occurrence at higher heights, in all three seasons, but in particular in summer. Also, the inter-annual variability is expected to increase significantly, with the exception of August.

The projected changes for the Western Iberian CLLJ are substantial and are in accordance with Wang et al. (2015) and Semedo et al. (2016), emphasizing the increased impacts at EBCS higher latitudes. Here, an explanation is proposed to understand the future evolution the main CLLJ ingredients, based on the changes in the main circulation ingredients, from the synoptic to the regional scales. In fact, in future climate, the Azorean Anticyclone is more persistent and its influence extends further northeast encompassing in a greater measure the areas to the north of Iberia, forcing more frequent and more intense along-shore winds, especially in the north sector of Iberia. At the same time, the ocean-land thermal contrast appears enhanced in the end of the twenty-first century, and again in a larger extent in the north part. These two CLLJ conditioning effects add to the general CLLJ augments mentioned. The future changes in the Iberian CLLJ may have a direct impact on the upper ocean properties and in the upwelling regime, and thus on the biological production. The enhancement of low-level jets would lead to an increased upwelling rate, greater turbulence in the upper-ocean, and faster offshore transport of surface waters (Bakun et al. 2015). These effects may be, however, counteracted by upper-ocean warming which could increase water column stratification. The interaction between the upwelled waters, thermocline depth, turbulent mixing and the strength of the wind jets is still an unresolved question (Bakun et al. 2015)

To our knowledge the current study is the first one using both high resolution and temporal sampling to address the signal of climate change on a relevant CLLJ system. The extension of this work to other CLLJs and the identification and attribution of the role of the changes on the regional climate it is a challenging and promising investigation for a near future. Obviously, the important feedbacks between the CLLJ and upwelling should be taken in account and a high resolution ocean–atmosphere coupled simulation would be desirable to analyse these feedbacks in present and future climates.

Acknowledgments This work was pursuit in the framework of the SOLAR Project (PTDC/GEOMET/7078/2014) and of the SHARE Project (RECI/GEO-MET/0380/2012), both financed by the Portuguese Foundation for Science and Technology (FCT). Daniela Lima was supported by FCT through a doctoral Grant PD/BD/106008/2014, within the EarthSystems Doctoral Programm of the Faculty of Sciences of the University of Lisbon. RM Cardoso was supported by EUPORIAS—7th Framework Programme for Research, Grant Agreement 308291. All authors are part of UID/GEO/50019/2013.

References

Alvarez I, Gomez-Gesteira M, deCastro M, Dias JM (2008) Spatiotemporal evolution of upwelling regime along the western coast of the Iberian Peninsula. J Geophys Res 113:C07020. doi:10.1029/2008JC004744

Bakun A (1990) Global climate change and intensification of coastal ocean upwelling. Science 247:198–201

Bakun A, Black BA, Bograd SJ, García-Reyes M, Miller AJ, Rykaczewski RR, Sydeman WJ (2015) Anticipated effects of climate change on coastal upwelling ecosystems. Curr Clim Chang Rep 1:85–93. doi:10.1007/s40641-015-0008-4

Balas N, Nicholson SE, Klotter D (2007) The relationship of rainfall variability in West central Africa to sea-surface temperature fluctuations. Int J Climatol 27:1335–1349

Beardsley RC, Dorman CE, Friehe CA, Rosenfield LK, Wynant CD (1987) Local atmospheric forcing during the coastal ocean dynamics experiment 1: a description of the marine boundary layer and atmospheric conditions over a Northern California upwelling region. J Geophys Res 92:1467–1488

Betts AK (1986) A new convective adjustment scheme. Part I: observational and theoretical basis. Q J R Meteorol Soc 112:677–691

Betts AK, Miller MJ (1986) A new convective adjustment scheme. Part II: single column tests using GATE wave, BOMEX, and arctic air-mass data sets. Q J R Meteorol Soc 112:693–709

Bravo M, Mira T, Soler MR, Cuxart J (2008) Intercomparison and evaluation of MM5 and Meso-NH mesoscale models in the stable boundary layer. Bound-Layer Meteorol 128(1):77–101. doi:10.1007/s10546-008-9269-y

Burk SD, Thompson WT (1996) The summertime low-level jet and marine boundary layer structure along the California coast. Mon Weather Rev 124:668–686

Campaniço H, Soares PMM, Hollmuller P, Cardoso RM (2016) Climatic cooling potential and building cooling demand savings: high resolution spatiotemporal analysis of direct ventilation and evaporative cooling for the Iberian Peninsula. Renew Energy 85:766–776. doi:10.1016/j.renene.2015.07.038

Cardoso RM, Soares PMM, Miranda PMA, Belo-Pereira M (2013) WRF high resolution simulation of Iberian mean and extreme precipitation climate. Int J Climatol 33:2591–2608. doi:10.1002/joc.3616

Cardoso RM, Soares PMM, Lima D, Semedo A (2016) The impact of climate change on the Iberian low-level wind jet: EURO-CORDEX regional climate simulation. Tellus A 68:29005. doi:10.3402/tellusa.v68.29005

Chen F, Dudhia J (2001) Coupling an advanced land surface-hydrology model with the Penn State-NCAR MM5 modelingsystem. Part I: model implementation and sensitivity. Mon Weather Rev 129:569–585

Collins WD et al (2004) Description of the NCAR Community Atmospheric Model (CAM 3.0). NCAR Tech. Note, NCAR/TN-4641STR, p 226

Cui Z, Tjernström M, Grisogono B (1998) Idealized simulations of atmospheric coastal flow along the central coast of California. J Appl Meteorol 37(10):1332–1363

Davis RE, Hayden BP, Gay DA, Phillips WL, Jones GV (1997) The North Atlantic subtropical anticyclone. J Clim 10:728–744

Dee DP, Uppala SM, Simmons AJ, Berrisford P, Poli P, Kobayashi S, Andrae U, Balmaseda MA, Balsamo G, Bauer P, Bechtold P, Beljaars ACM, van de Berg L, Bidlot J, Bormann N, Delsol C, Dragani R, Fuentes M, Geer AJ, Haimberger L, Healy SB, Hersbach H, Hólm EV, Isaksen L, Kållberg P, Köhler M, Matricardi M, McNally AP, Monge-Sanz BM, Morcrette JJ, Park BK, Peubey C, de Rosnay P, Tavolato C, Thépaut JN, Vitart F (2011) The ERA-Interim reanalysis: configuration and performance of the data assimilation system. Q J R Meteorol Soc 137:553–597. doi:10.1002/qj.828

Dorman CE, Beardsley RC, Limeburner R (1995) Winds in the strait of Gibraltar. Q J R Meteorol Soc 121:1903–1921
Douglas MW (1995) The summertime low-level jet over the Gulf of California. Mon Weather Rev 123:2334–2347
Findlater J (1969) A major low level current near the Indian Ocean during northern 686 summer. Q J R Meteorol Soc 95:362–380
Garreaud RD, Muñoz RC (2005) the low-level jet off the west coast of subtropical South America: structure and variability. Mon Weather Rev 133:2246–2261
Garreaud RD, Rutllant JA, Muñoz RC, Rahn DA, Ramos M, Figueroa D (2011) VOCALS-CUpEX: the chilean upwelling experiment. Atmos Chem Phys 11:2015–2029. doi:10.5194/acp-112015-2011
Goddard L, Graham NE (1999) Importance of the Indian Ocean for simulating rainfall anomalies over eastern and southern Africa. J Geophys Res 104(D16):19099–19116
Hazeleger W et al (2010) EC-Earth: a seamless earth system prediction approach in action. BAMS 91:1357–1363
Helfand HM, Schubert SD (1995) Climatology of the simulated great plains low-level jet and its contribution to the continental moisture budget of the United States. J Clim 8:784–806
Hoinka KP, de Castro M (2003) The Iberian Peninsula thermal low. Q J R Meteorol Soc 129:1491–1511. doi:10.1256/qj.01.189
Hong S-Y, Lim J-OJ (2006) The WRF single-moment 6-class microphysics scheme (WSM6). J Korean Meteorol Soc 42:129–151
Hu X-M, Nielsen-Gammon JW, Zhang F (2010) Evaluation of three planetary boundary layer schemes in the WRF model. J Appl Meteorol Climatol 49:1831–1844
Janjic ZI (1990) The step-mountain coordinate: physical package. Mon Weather Rev 118:1429–1443
Janjic ZI (1994) The step-mountain eta coordinate model: further developments of the convection, viscous sublayer and turbulence closure schemes. Mon Weather Rev 122:927–945
Janjic ZI (2000) Comments on "development and evaluation of a convection scheme for use in climate models". J Atmos Sci 57:3686
Janjic ZI (2001) Nonsingular implementation of the Mellor–Yamada level 2.5 scheme in the NCEP Meso Model. NCEP Office Note 437, p 61
Lamb PJ, Peppler RA (1992) Further case studies of Tropical Atlantic surface atmospheric and oceanic patterns associated with sub-Saharan drought. J Clim 5:476–488
Lettau H (1978) Explaining the world's driest climate. In: Lettau HH, Lettau K (eds) Exploring the world's driest climate. University of Wisconsin, Madison, pp 182–248
Li W, Li L, Ting M, Liu Y (2012) Intensification of Northern Hemisphere subtropical highs in a warming climate. Nat Geosci 5:830–834. doi:10.1038/ngeo1590
Magarreiro C, Cardoso RM, Widmann M, Brito MC, Soares PMM (2016) Combining high resolution dynamical downscaling and quantile mapping for future projections of the Iberian solar resource. Int J Climatol **(accepted)**
Martins JPA, Cardoso RM, Soares PMM, Trigo IF, Belo-Pereira M, Moreira N, Tomé R (2015) The summer diurnal cycle of coastal cloudiness over west Iberia using Meteosat/SEVIRI and a WRF regional climate model simulation. Int J Climatol. doi:10.1002/joc.4457
Miranda PMA, Alves JMR, Serra N (2013) Climate change and upwelling: response of Iberian upwelling to atmospheric forcing in a regional climate scenario. Clim Dyn 40:2813–2824. doi:10.1007/s00382-012-1442-9
Monteiro IT, Santos AJ, Belo-Pereira M, Oliveira PB (2016) Adjustment of the summertime marine atmospheric boundary layer to the western Iberia coastal morphology. J Geophys Res Atmos. doi:10.1002/2016JD025055
Moss RH, Edmonds JA, Hibbard KA, Manning MR, Rose SK, van Vuuren DP, Carter TR, Emori S, Kainuma M, Kram T et al (2010) The next generation of scenarios for climate change research and assessment. Nature 463:747–756
Nicholson SE (2010) A low-level jet along the Benguela coast, an integral part of the Benguela current ecosystem. Clim Chang 99:613–624
Nicholson SE, Entekhabi D (1987) Rainfall variability in equatorial and Southern Africa: relationships with sea-surface temperatures along the southwestern coast of Africa. J Clim Appl Meteorol 26:561–578
Nicholson SE, Webster PJ (2007) A physical basis for the interannual variability of rainfall in the Sahel. Q J R Meteorol Soc 133:2065–2084
Overland JE (1984) Scale analysis of marine winds in straits and along mountainous coasts. Mon Weather Rev 112:2530–2534
Parish TR (2000) Forcing of the summertime low-level jet along the California coast. J Appl Meteorol 39:2421–2433
Pomeroy KR, Parish T (2001) A case study of the interaction of the summertime coastal jet with the California topography. Mon Weather Rev 129:530–539
Ranjha R, Svensson G, Tjernström M, Semedo A (2013) Global distribution and seasonal variability of coastal low-level jets derived from ERA-Interim reanalysis. Tellus A 65:20412
Ranjha R, Tjernström M, Semedo A, Svensson G, Cardoso RM (2015) Structure and variability of the Oman coastal low-level jet. Tellus A 67:25285. doi:10.3402/tellusa.v67.25285
Reason CJC, Rouault M (2006) Sea surface temperature variability in the tropical southeast Atlantic Ocean and West African rainfall. Geophys Res Lett 33:L21705. doi:10.1029/2006GL027145
Relvas P, Barton ED (2002) Mesoscale patterns in the Cape São Vicente (Iberian Peninsula) upwelling region. J Geophys Res 107(C10):3164. doi:10.1029/2000JC000456
Renault L, Dewitte B, Falvey M, Garreaud R, Echevin V, Bonjean F (2009) Impact of atmospheric coastal jet off central Chile on sea surface temperature from satellite observations (2000–2007). J Geophys Res 114:C08006. doi:10.1029/2008JC005083
Riahi K, Rao S, Krey V, Cho C, Chirkov V, Fisher G, Kindermann G, Nakicenovic N, Rafaj P (2011) RCP8.5—a scenario of comparatively high greenhouse gas emissions. Clim Chang 109:33–57. doi:10.1007/s10584-011-0149-y
Rios-Entenza A, Soares PMM, Trigo RM, Cardoso RM, Miguez-Macho G (2014) Moisture recycling in the Iberian Peninsula from a regional climate simulation: spatiotemporal analysis and impact on the precipitation regime. J Geophys Res Atmos 119:5895–5912. doi:10.1002/2013JD021274
Semedo A, Soares PMM, Lima DCA, Cardoso RM, Bernardino M, Miranda PMA (2016) The impact of climate change on the global low-level wind jets: EC-EARTH simulations. Glob Planet Chang 137:88–106. doi:10.1016/j.gloplacha.2015.12.012
Skamarock WC, Klemp JB, Dudhia J, Gill DO, Barker DM, co-authors (2008) A description of the advanced research WRF Version 3. NCAR Tech Note TN-468 + STR 113 pp
Snyder MA, Sloan LC, Diffenbaugh NS, Bell JL (2003) Future climate change and upwelling in the California current. Geophys Res Lett 30:1823. doi:10.1029/2003GL017647
Soares PMM, Cardoso RM, Miranda PMA, Medeiros J, Belo-Pereira M et al (2012) WRF high resolution dynamical downscaling of ERA-Interim for Portugal. Clim Dyn 39:2497–2522
Soares PMM, Cardoso RM, Semedo A, Chinita MJ, Ranjha R (2014) Climatology of Iberia coastal low-level wind jet: WRF high resolution results. Tellus A 66:22377
Soares PMM, Cardoso RM, Lima DCA, Miranda PMA (2016) Future precipitation in Portugal: high resolution regional climate simulation projections. Clim Dyn **(accepted)**
Stensrud DJ (1996) Importance of low-level jets to climate: a review. J Clim 9:1698–1711

Tjernström M (1999) The sensitivity of supercritical atmospheric boundary-layer flow along a coastal mountain barrier. Tellus 51A:880–901

Tomczak M, Godfrey JS (1994) Regional oceanography: an introduction. Pergamon, Oxford, p 442

Torres R, Barton ED, Miller P, Fanjul E (2003) Spatial patterns of wind and sea surface temperature in the Galician upwelling region. J Geophys Res 108(C4):3130. doi:10.1029/2002JC001361

van Vuuren DP, Edmonds J, Kainuma M et al (2011) The representative concentration pathways: an overview. Clim Chang 109:5. doi:10.1007/s10584-011-0148-z

Wang D, Gouhier TC, Menge BA, Ganguly AR (2015) Intensification and spatial homogenization of coastal upwelling under climate change. Nature 518:390–394

Webster PJ, Hoyos C (2004) Prediction of monsoon rainfall and river discharge on 15–30 day time scales. Bull Am Meteorol Soc 85(11):1745–1765

Winant CD, Dorman CE, Friehe CA, Beardsley RC (1988) The marine layer off Northern California: an example of supercritical channel flow. J Atmos Sci 45:3588–3605